

A study of viscosity inhomogeneity in porous media

E. Akhmatkaya^{a)}

School of Chemical Engineering, Cornell University, Ithaca, New York 14853

B. D. Todd,^{b)} P. J. Davis,^{c)} and D. J. Evans

Research School of Chemistry, Australian National University, Canberra, ACT 0200 Australia

K. E. Gubbins and L. A. Pozhar^{d)}

School of Chemical Engineering, Cornell University, Ithaca, New York 14853

(Received 10 October 1996; accepted 13 December 1996)

The theory of transport in highly inhomogeneous systems, developed recently by Pozhar and Gubbins, and the nonequilibrium molecular dynamics (NEMD) technique are employed to study the viscosity of WCA fluids confined in narrow slit pores of width 5.1 and 20σ at reduced densities $\rho\sigma^3$ of 0.422–0.713. Calculated quantities include the equilibrium and nonequilibrium density profiles, equilibrium pair correlation functions, flow velocity profiles, and the viscosity profiles. NEMD simulation results are compared with the theoretical predictions. The agreement is good except for the region within one molecular diameter from the walls. The viscosity was found to vary with position across the pore. © 1997 American Institute of Physics. [S0021-9606(97)50911-1]

I. INTRODUCTION

There has been much progress in the last decade in understanding the equilibrium properties (adsorption, phase transitions, isosteric heats, solvation forces, etc.) of fluids confined in narrow pores; much of the advance has derived from the application of density functional theory and molecular simulation applied to model fluid/pore systems. Much less work has been reported on transport processes in such confined systems.^{1–3} From the experience with equilibrium properties, we might anticipate that approaches based on continuum hydrodynamics, or on bulk-phase kinetic equations plus boundary conditions, are likely to break down for micro- and meso-pores. A molecular understanding of fluid flow near solid surfaces and in pores is needed to understand the mechanisms involved in lubrication, pressure driven flow in porous media (e.g., in tertiary oil recovery), friction, and spreading. Davis^{4,5} developed a kinetic theory of transport in inhomogeneous fluids by extending the revised Enskog theory, but obtained transport coefficients only for the case of a local equilibrium velocity distribution, with inhomogeneity in one direction; his theory involved an *ad hoc* approximation, namely the replacement of the pair correlation function for the inhomogeneous fluid by the corresponding function for the homogeneous fluid at a certain smoothed density. Pozhar and Gubbins^{1,2} have recently presented a more rigorous theory for transport in inhomogeneous fluids, which is a generalization of the modified Enskog theory of

Sung and Dahler⁶ for homogeneous fluids. This theory, which treats an atomic fluid in which the pair potentials are made up of a hard core and a soft part, relies on the 13-moment approximation and neglects dynamic memory effects (particularly repeated core collisions), as in the Sung–Dahler theory. Based on experience with homogeneous fluids, it seems reasonable to hope that these approximations would not lead to large errors. The resulting equations are tractable, and relate local values of the transport coefficients to integrals over the *equilibrium* inhomogeneous fluid singlet and pair correlation functions; only the pair correlation function at core contact is needed. The transport coefficient expressions are nonlocal, since the value of the coefficient at some point z , say, involves the density and pair correlation function at other nearby locations. These equations have not yet been tested.

The purpose of this paper is to report a nonequilibrium molecular dynamics (NEMD) study of planar Poiseuille flow in model slit pores, together with a test of the Pozhar–Gubbins theory. In particular, we study how the viscosity varies in the vicinity of the pore wall due to confinement. Davis and co-workers^{7–10} have previously reported NEMD results for flow in pores, but did not obtain local viscosities. In Sec. II we briefly summarize the model used for the fluid and pore. The theoretical equations and simulation methods are described in Sec. III. Results are presented and discussed in Sec. IV, and conclusions made in Sec. V.

II. MODEL

Both the fluid–fluid and fluid–wall interactions are modeled with the Weeks–Chandler–Andersen (WCA) repulsive potential,

$$\begin{aligned}\phi(r) &= 4\epsilon \left[\left(\frac{\sigma}{r} \right)^{12} - \left(\frac{\sigma}{r} \right)^6 \right] + \epsilon, \quad r < 2^{1/6}\sigma \\ &= 0, \quad r \geq 2^{1/6}\sigma.\end{aligned}\quad (1)$$

^{a)}Current address: Department of Chemistry, University of Manchester, Oxford Road, Manchester M13 9PL, U.K.

^{b)}Current address: Cooperative Research Center for Polymers, c/o CSIRO Division of Chemicals and Polymers, Private Bag 10, Rosebank MDC, Clayton, Victoria 3169, Australia.

^{c)}Current address: Department of Applied Physics, Royal Melbourne Institute of Technology, GPO Box 2476V, Melbourne, Victoria 3001, Australia.

^{d)}Permanent address: Institute for Low Temperature Physics and Engineering, National Academy of Sciences of the Ukraine, 47 Lenin Avenue, Kharkov 310164, Ukraine.

We take the fluid–fluid and fluid-wall potential parameters to be the same, and in what follows we set the σ and ϵ parameters equal to unity. The atomic mass is also set equal to unity.

The fluid was confined between parallel, structured walls. Two pore widths were studied, $H=5.1$ and $H=20$ in units of σ . Pore width was defined as the distance between the two planes through the centers of the surface layer of wall atoms for the opposing walls (see Fig. 1). Each wall consisted of three layers of atoms arranged in a fcc lattice structure; there were 72 atoms per layer for $H=5.1$ (a total of 216 wall atoms), and 18 atoms per layer for $H=20$ (54 wall atoms total).

In the theoretical calculations (and the simulations needed to obtain the equilibrium correlation functions) the wall atoms were fixed in space, since the theory was developed for this case. In the NEMD simulations, however, the wall atoms were tethered to lattice sites by a simple harmonic potential. This restoring potential is applied to each atom, and is that suggested by Powles *et al.*,¹¹

$$\phi_{Ti}(r) = \frac{1}{2} K(r_i - r_{ei})^2, \quad (2)$$

where r_i and r_{ei} are the instantaneous and equilibrium positions of wall atom i , and K is a spring constant. A possible problem with such a restoring potential is that fluid pressure can cause an increase in pore width,¹² so that the pore width and volume can vary with the flow rate. In order to avoid this problem we have developed¹³ a constraining mechanism, based on Gauss' principle of least constraint,¹⁴ which keeps

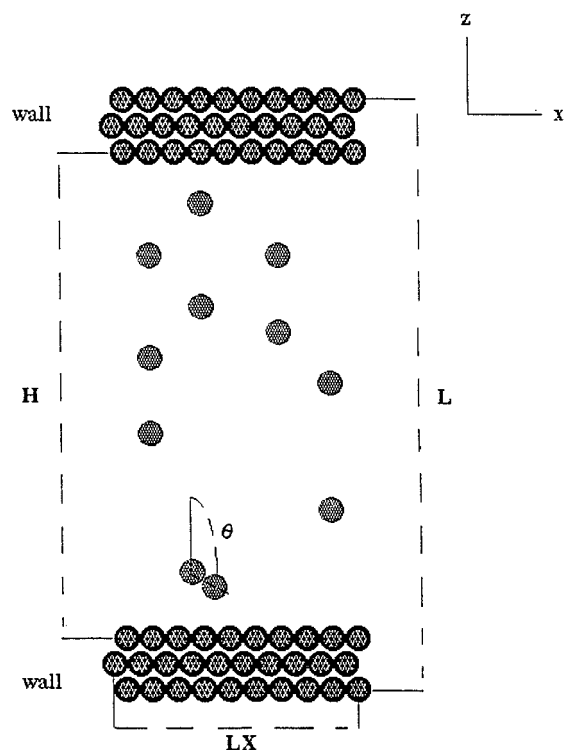


FIG. 1. Slit pore geometry used in simulation studies.

the z coordinate (z is the direction normal to the wall) of the center of mass of each of the atomic wall layers constant. Since the steady-state Poiseuille flow produces viscous heat, we thermostat the walls by a method that also invokes Gauss' principle of least constraint. The excess heat is removed from the fluid by heat conduction to the thermostatted walls. The technique is well known and described in detail elsewhere.^{13,14} The wall temperature was fixed at $T_w=0.722$.

III. METHODS

A. Theory

The final expression for the viscosity coefficient in the Pozhar–Gubbins theory² has a simple and tractable structure,

$$\eta_{\text{slit}}^*(z) = 4\pi n^*(z)\tau_\eta^*(z)(1 + \pi\beta^{*0}(z))^2 + (16/5)\pi\beta^{*0}(z)n^*(z). \quad (3)$$

Here $\eta_{\text{slit}}^*(z) = \eta_{\text{slit}}(z)/\eta$ is the reduced local viscosity, $\eta = (5/16\sigma^2)(m/\pi\beta)^{1/2}$ is the viscosity of a dilute hard sphere gas, $\beta = 1/(k_B T)$, m is the mass of a fluid molecule, σ is the hard-core diameter, $n^*(z) = n(z)\sigma^3$ is the equilibrium reduced number density, and

$$\tau_\eta^*(z) = [2\pi(v^*(z) + 1/3v_1^*(z) + \sqrt{2}v_2^*(z))]^{-1}, \quad (4)$$

$$\beta^{*0}(z) = \int_0^\pi \sin^3 \theta \cos^2 \theta n^*(z - \sigma \cos \theta) \times g(z, z - \sigma \cos \theta) d\theta, \quad (5)$$

$$v^*(z) = \int_0^\pi \sin \theta n^*(z - \sigma \cos \theta) g(z, z - \sigma \cos \theta) d\theta, \quad (6)$$

$$v_1^*(z) = \int_0^\pi \sin \theta [n^*(z - \sigma \cos \theta) - n^*(z)] \times g(z, z - \sigma \cos \theta) d\theta, \quad (7)$$

$$v_2^*(z) = \int_0^\pi \sin \theta n_w^*(z - \sigma_{1w} \cos \theta) \times g_w(z, z - \sigma_{1w} \cos \theta) d\theta, \quad (8)$$

where $g(z, z - \sigma \cos \theta)$ is the equilibrium pair correlation function contact value, z is the coordinate in the direction orthogonal to the pore wall, and θ is the angle between the intermolecular vector and the positive z direction; $n_w^*(z)$, $g_w(z, z - \sigma_{1w} \cos \theta)$, and σ_{1w} are the equilibrium wall molecule number density, the fluid-wall pair correlation function contact value, and the hard core diameter for a fluid molecule in contact with the wall, respectively.

In the following we will omit the notation “*”, assuming all quantities in use are reduced.

The viscosity coefficients can be calculated immediately provided the equilibrium number density $n(z)$, the equilib-

TABLE I. Parameters for MD simulations.

Simulation box sizes		Pore width, H	Fluid av. number density, n_{av}^f	Wall av. number density, n_{av}^w	Temperature T	Number of fluid mol., N_f	Number of wall mol., N_w
L	$LX=LY$						
8.2836	12.635	5.1	0.442	0.85	0.729	360	216
8.8624	11.622	5.1	0.522	0.85	0.755	360	216
9.4412	10.82	5.1	0.603	0.85	0.958	360	216
22.6692	6.8196	20	0.523	0.87	1.382	486	54
23.1546	6.2732	20	0.618	0.87	1.254	486	54
23.6398	5.84	20	0.713	0.87	1.179	486	54

rium pair correlation function contact value $g(z, z - \sigma \cos \theta)$, and the hard-core diameter are known for the composite potential:

$$\phi = \phi_H + \phi_{\text{soft}}, \quad (9)$$

where ϕ_H and ϕ_{soft} denote hard core repulsive and soft attractive contributions, respectively.

In order to check these theoretical results we need to calculate the contact values of the equilibrium inhomogeneous pair correlation function as a function of two variables, z and θ . To collect the proper statistics for inhomogeneous distribution function evaluation we need to simulate the system with a large number of molecules for a long time period.

B. Equilibrium MD simulation method

In order to determine the density profiles and pair correlation functions needed in the theory, we carried out equilibrium MD simulations for a system of WCA atoms confined by parallel walls. Pore widths were taken to be 5.1 and 20 fluid atomic diameters (σ) apart. We performed simulations for three different average number densities for each pore size. The average fluid density is defined as

$$n_{av}^f = N_f / V_f, \quad (10)$$

where N_f is the number of fluid atoms and V_f is the volume of the fluid, $V_f = H \times LX \times LY$. Here H is the pore width, defined as the distance between the surface layer of the molecules of the upper wall and the first layer of the molecules of the lower wall. LX, LY are the sizes of the simulation box in the x and y directions. For the calculation of the average wall density we used the expression

$$n_{av}^w = N_w / V_w, \quad (11)$$

where N_w is the number of wall molecules, V_w is the wall volume, $V_w = (L - H) \times LX \times LY / 2$, and L denotes the size of the simulation box in the z direction. The simulation parameters are summarized in Table I.

For the MD simulations we used Verlet's leapfrog algorithm¹⁵ to solve the equations of motion with a time step of 8×10^{-3} . The periodic boundary conditions were applied in two directions: x and y . We discarded the first 50 000 equilibrium MD time steps and then performed equilibrium MD for 950 000 time steps. The density profile was calcu-

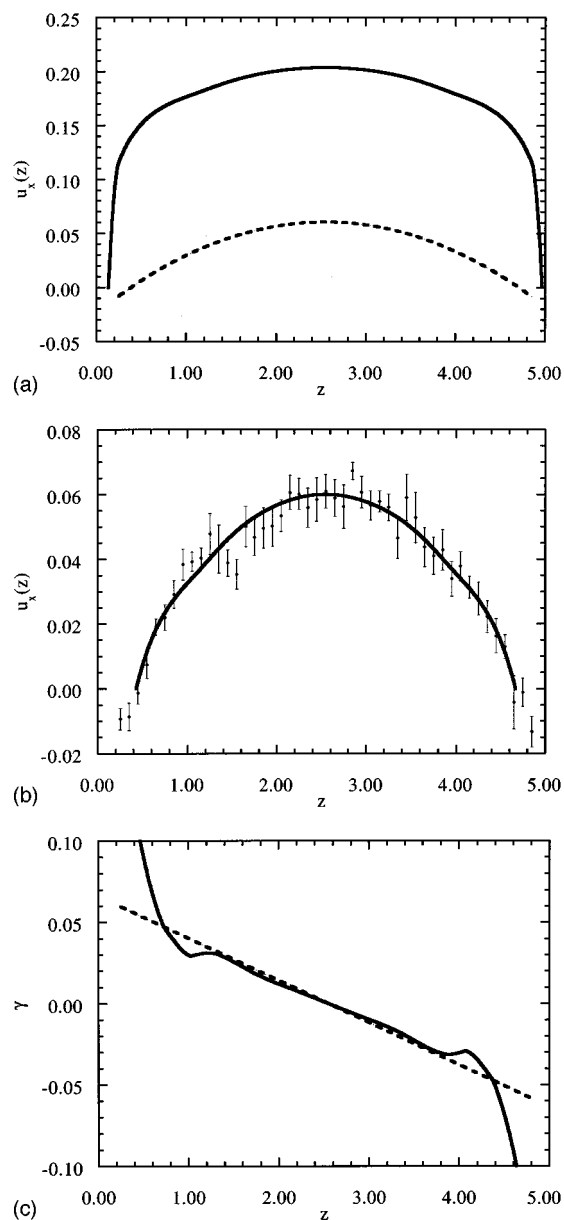


FIG. 2. Comparison of theory (solid lines) and NEMD results (dashed lines and points) for a pore of reduced width $H=5.1$, average reduced density $n_{av}^f=0.442$, and average reduced temperature $T=0.729$: (a) velocity profiles; (b) velocity profiles after matching theoretical values to NEMD at mid-channel (see text); (c) strain rates.

lated by dividing the pore into bins of width Δz along the z axis, and accumulating a histogram of the number of molecules, N_i , in each bin.

In calculating the pair correlation function $g(z, z - \sigma \cos \theta)$ needed in Eqs. (5)–(8), we used the assumption that the molecules have collided if the distance between them is less than $1.0005\sigma_d$, where σ_d is a hard-core diameter. To choose the hard-core diameter σ one can use the Weeks, Chandler, and Anderson (WCA)¹⁶ or Barker and Henderson (BH)¹⁷ methods. The WCA method supplies a hard-core diameter, σ_{WCA} , which depends on the equilibrium number density and temperature of the fluid, whereas the BH procedure yields σ_{BH} which depends only on temperature. The BH choice of hard-core diameter is much more attractive for inhomogeneous fluids, because σ_{BH} does not depend on the density of the fluid. Making this choice we do not need to calculate σ for each local value of $n(z)$, as in the case of σ_{WCA} .

In this paper we present results for the viscosity coefficient calculation with the use of σ_{BH} . The hard-core diameter σ_{BH} was obtained numerically from the expression

$$\sigma_{\text{BH}} = \int_0^{r_m} \{1 - \exp[-\beta\phi(z)]\} dz, \quad (12)$$

where $r_m = 2^{1/6}\sigma$, and $\phi(z)$ is the WCA potential. For our model $\sigma = \sigma_{1w} = \sigma_{\text{BH}}$.

We mention one more problem complicating the accurate calculation of the pair correlation function contact value. This arises from the uncertainty of the position in the pore of the contact molecule. The z position of such molecules is defined as $z - \sigma \cos \theta$. However, because of the histogram method used, the error in defining $z - \sigma \cos \theta$ can be up to $\Delta z - \sigma\Delta\theta$. Such errors can be reduced by using a large number of time steps. Ideally, if one molecule belongs to the i th bin on z , then another one from the collision pair must have as its z position:

$$z = z_i - \sigma \cos \theta_j, \quad (13)$$

where z_i is the center of the i th bin and θ_j gives the center of the j th bin. To test the statistics we defined the position of the contact molecule in two different ways. One of them was direct, using (13). Another was to accumulate z positions of the contact molecules during simulations, and then to average over the number of contact molecules and the number of time steps. Thus, we found the optimal number of time steps is 950 000. Also, to improve the accuracy of the $g(z, z - \sigma \cos \theta)$ calculation we averaged the results over both ends of the simulation box, as the two walls are independent.

The fluid pair correlation function at ‘‘contact’’ was calculated using the histogram method, and (for sufficiently small Δz and $\Delta\theta$) is given by

$$g(z, z - \sigma \cos \theta) = 2\langle N_{12} \rangle / (n(z)n(z - \sigma \cos \theta)V_1V_2), \quad (14)$$

where V_1 is the volume of the bin centered at z , V_2 is the volume occupied by the bin containing collision partners of molecule 1 at angles between θ and $\theta + d\theta$, and $\langle N_{12} \rangle$ is the average number of contact molecules, one of which lies in

the bin at z , and the other in the bin corresponding to contact and angle θ . The calculation of V_2 is tedious but straightforward. Care must be taken to distinguish the cases $\theta \leq \pi/2$, $\theta > \pi/2$, $\theta + \Delta\theta > \pi/2$. In our simulations we used $\Delta z = 0.1$ and $\Delta\theta = 0.01$.

Although there exists a variety of contributions to the viscosity due to the presence of walls, the main contribution is that from $\nu_2(z)$. As follows from Eq. (8), this contribution is proportional to

$$\int_0^\pi \sin \theta n_w(z - \sigma_{1w} \cos \theta) g_w(z, z - \sigma_{1w} \cos \theta) d\theta$$

and is nonzero only for distances l from the walls of about σ_{1w} or less. However, for separations $l \sim \sigma_{1w}$ the values of $\nu_2(z)$ can differ significantly from those for $l > \sigma_{1w}$. Since both functions $n_w(z - \sigma_{1w} \cos \theta)$ and $g_w(z, z - \sigma_{1w} \cos \theta)$ are positive, the values of $\tau_\eta(z)$ at $l = \sigma_{1w}$ could be smaller than those at $l > \sigma_{1w}$. This could lead to a decrease of viscosities at distances $l \sim \sigma_{1w}$ from the walls. Thus, we cannot neglect the term $\nu_2(z)$. To obtain this term we calculated $g_w(z, z - \sigma_{1w} \cos \theta)$ using

$$g_w(z, z - \sigma_{1w} \cos \theta) = 2\langle N_{wf} \rangle / (n(z)n_w(z - \sigma_{1w} \cos \theta)V_1V_2). \quad (15)$$

Here $\langle N_{wf} \rangle$ is the average number of pairs of contacting molecules, one of which is a fluid molecule from the bin of width Δz centered at z , and the other is a wall molecule; the angle between \mathbf{r}_{12} and the positive z direction lies in the range $[\theta, \theta + \Delta\theta]$, $n(z)$ is the fluid number density at z , and $n_w(z - \sigma_{1w} \cos \theta)$ corresponds to the wall number density.

All integrals in Eqs. (5)–(8) were computed using the composite trapezoid rule.¹⁸

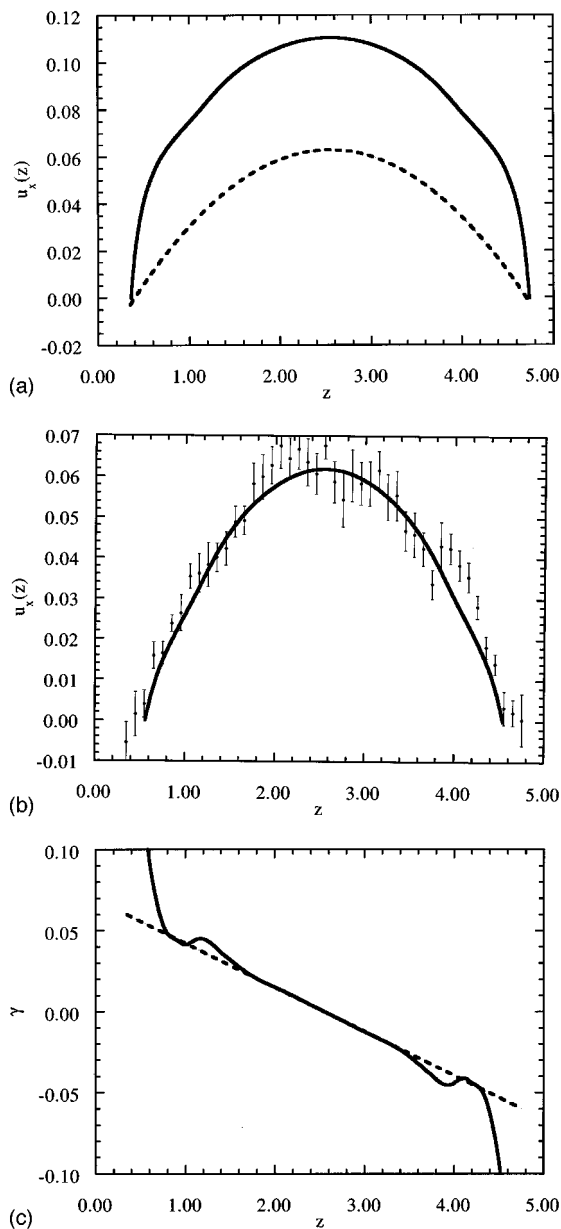
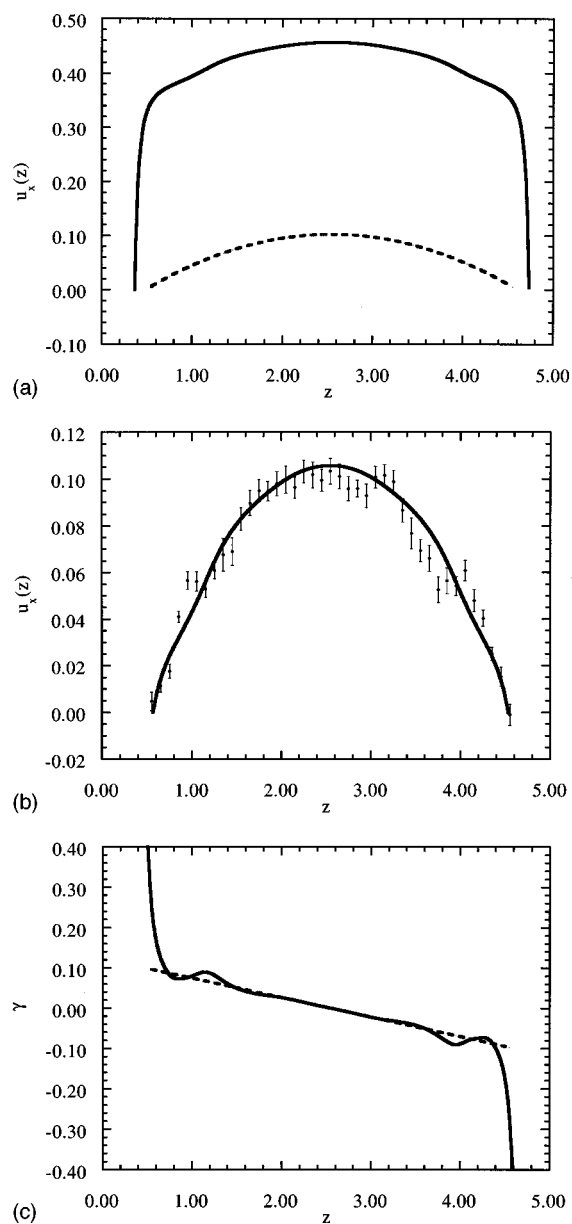
C. NEMD method

In addition to the theory above, the fluid viscosity was also calculated directly by NEMD simulations of a fluid undergoing planar Poiseuille flow for channels of width $H = 5.1$ and $H = 20.0$. In a previous paper¹³ it was shown that the shear stress for a nonequilibrium fluid under simulated planar Poiseuille flow may be determined by either the so-called method of planes (MOP) technique, or the statistically superior mesoscopic route of directly integrating the momentum continuity equation of hydrodynamics (which we call the IMC technique). For the simulations performed in this work, we used the IMC technique to calculate the shear stress [i.e., $-P_{xz}(z)$]. For the geometry employed in the simulation, the local viscosity is defined by the expression,

$$\eta(z) = \lim_{F_e \rightarrow 0} - \frac{\langle P_{xz}(z) \rangle}{\gamma(z)}, \quad (16)$$

where $\langle \dots \rangle$ denotes ensemble or time average, and $\gamma(z)$ is the strain rate given by

$$\gamma(z) = \frac{\partial u_x(z)}{\partial z}. \quad (17)$$

FIG. 3. As for Fig. 2 but at $n_{av}=0.522$, $T=0.755$.FIG. 4. As for Fig. 2 but at $n_{av}=0.603$, $T=0.958$.

Here $u_x(z)$ is the streaming velocity of the fluid in the x direction, which is assumed to be quadratic.¹³ In the IMC method, $\langle P_{xz}(z) \rangle$ is given as

$$\langle P_{xz}(z) \rangle = F_e \int_0^z dz' n(z'), \quad (18)$$

where F_e is the driving force field (in the x direction) and $n(z')$ is the number density of the fluid.

The value of the spring constant in Eq. (2) for the restoring potential for wall atoms was taken to be $K=160$. This value was arrived at by trial. If K is much smaller than 160 fluid molecules can penetrate the wall, while if it is significantly larger momentum exchange with the wall becomes poor, and the fluid heats up too much.

The simulation cell was periodic in all three dimensions. There was only one three layer wall per simulation cell. The second wall is the periodic image of the first wall. This periodicity also ensures that the total density of the system remains constant. The simulations were performed using a fifth order Gear predictor-corrector scheme with an integrating timestep of $\tau=0.001$. Simulations were carried out for the two pore widths, each at three different system densities, where the fluid and wall densities are defined by Eqs. (10) and (11). The simulation parameters are given in Table I, and all simulations were run at a constant wall temperature of 0.722. For each pore width and each density, a set of 10 independent simulations of 100 000 timesteps each was carried out and averages taken of the quantities of interest. For further details of the simulation techniques used, and the

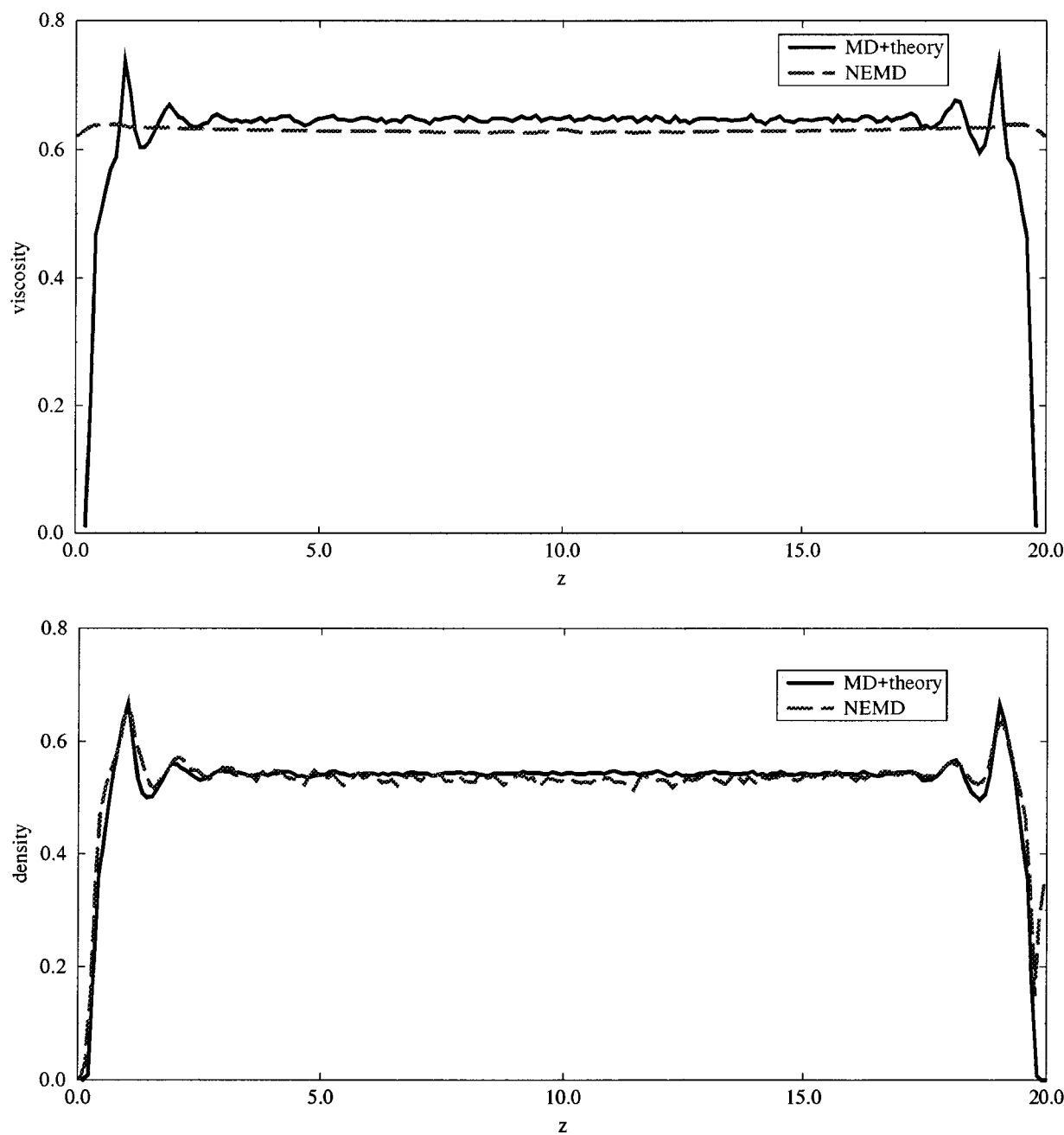


FIG. 5. Comparison of theory (solid lines) and NEMD results (dashed lines) for a pore of reduced width $H=20$, average reduced density $n_{av}=0.5225$ and reduced temperature $T=1.382$, showing reduced viscosity and density profiles across the pore.

equations of motion solved, the reader is referred to Ref. 13.

We note here that the NEMD viscosities calculated near the center of the pores need to be interpreted cautiously. Clearly, as the pore center is approached both P_{xz} and $\gamma(z) \rightarrow 0$, which leads to increasing uncertainty in $\eta(z)$, even if the statistics are reasonably good. Even slight fluctuations can lead to exaggerated values of $\eta(z)$ in the central pore regions. This uncertainty can of course be reduced, but not eliminated, by performing larger simulations to improve the statistics.

IV. RESULTS AND DISCUSSION

In this section we present the results of the NEMD simulations and theoretical calculations, and compare the two sets of results. Such comparisons are not completely straightforward. The theoretical expression for the local viscosity is for a fluid close to the equilibrium state, with small temperature gradients; the viscosity extracted from the NEMD simulation is for a flowing fluid with finite density and temperature

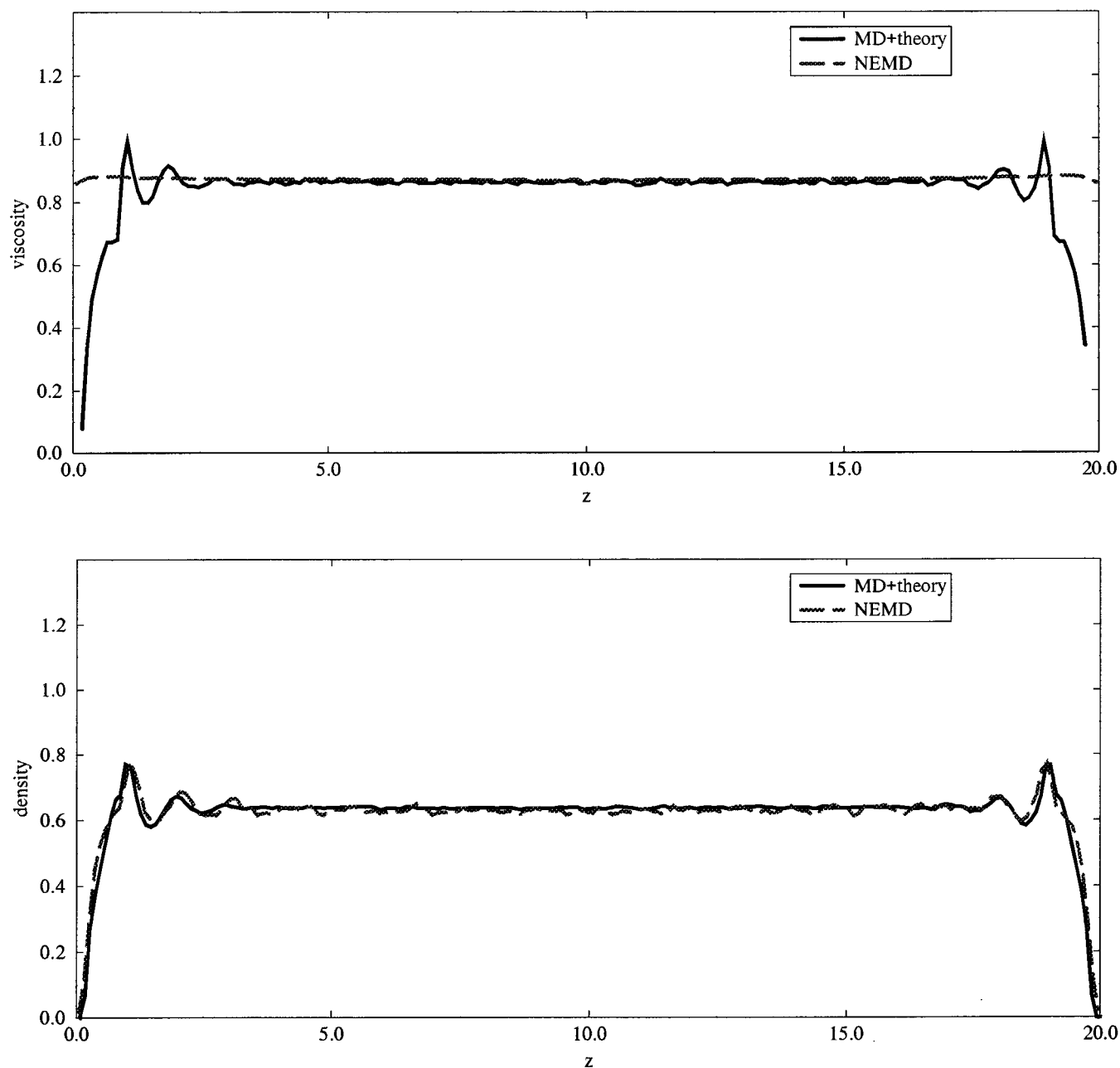


FIG. 6. As for Fig. 5, but for $n_{av}=0.6175$, $T=1.254$.

gradients. We note that, for a given pore width H , the shear viscosity is a complex function of temperature, density and strain rate,

$$\langle P_{xz}(r) \rangle = - \int dr' \eta(r, r-r'; T(r), \rho(r)) \gamma(r'). \quad (19)$$

We do not have sufficient information to calculate this viscosity kernel in our NEMD simulations. For Poiseuille flow in a parallel slit pore it is therefore convenient to define an effective viscosity $\eta(z)$:

$$\eta(z) = - \frac{\langle P_{xz} \rangle}{\gamma(z)}. \quad (20)$$

Both $P_{xz}(z)$ and $\gamma(z)$ obviously depend on the pressure head, but in the small strain limit $\eta(z)$ should be independent of the pressure head.

For this fixed flow geometry $\eta(z)$ is convenient for comparison purposes. However, because it ignores the full spatial convolution given in Eq. (19), we cannot expect $\eta(z)$ to be useful for comparisons of the viscosity with flows of the same fluid in different geometries (e.g., cylindrical pores).

In Figs. 2–4 we compare the streaming velocity profiles and strain rates obtained from NEMD and theory, for slit pores of $H=5.1$ for three different mean densities in the pore. The results are given for values of the reduced external

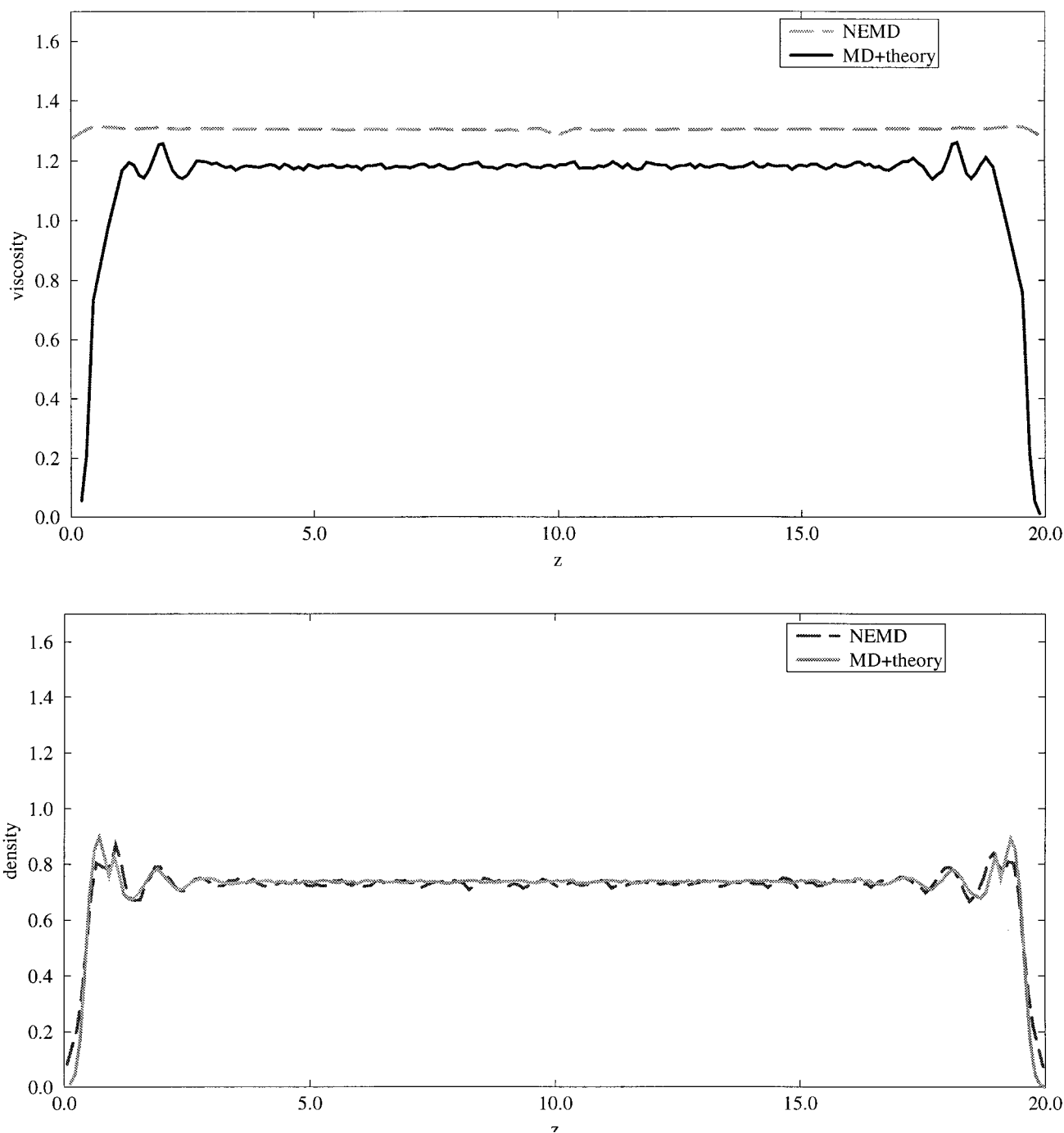


FIG. 7. As for Fig. 5, but for $n_{av}=0.7125$, $T=1.179$.

field that are close to zero; $F_e=0.02$, 0.03 , and 0.07 in Figs. 2, 3, and 4, respectively. The theoretical flow velocity profiles were obtained in the following fashion. Equation (18) was used to compute the shear stress as a function of z from a number density profile obtained from equilibrium MD. In the zero field ($F_e \rightarrow 0$) limit, induced changes to the number density do not affect the shear stress. The shear stress so obtained is essentially exact, in that the only errors result from errors in the equilibrium number density. This number density can be obtained to arbitrary accuracy from MD or

experiment. We note that in the small field limit, both the temperature and the density gradients vary as γ^2 .

Once the theoretical shear stress is known we substitute the theoretical $\eta(z)$ values calculated from Eq. (3) into the constitutive Eq. (16), and solve for the strain rate $\partial u_x / \partial z \equiv \gamma$. It is a trivial matter to finally integrate (17) to obtain the streaming velocity profile, $u_x(z)$; it is assumed that $u_x(\pm L)=0$. A comparison of the theoretical and NEMD velocity profiles so obtained is given in part (a) of Figs. 2–4. In these figures we immediately see that the theoretical velocity

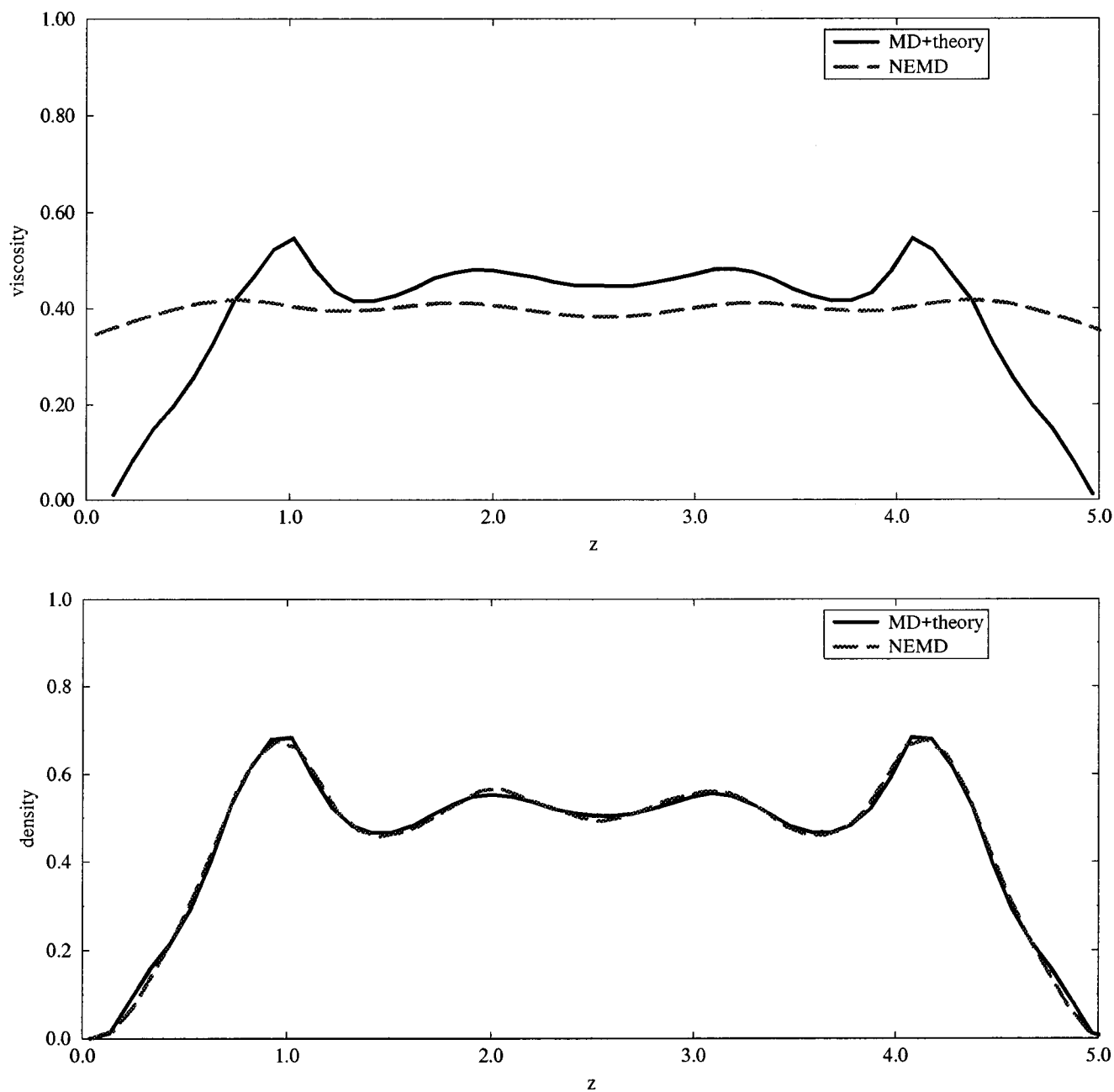


FIG. 8. As for Fig. 5, but for $H=5.1$, $n_{av}=0.442$, $T=0.729$.

profiles resemble those for “plug” flows. This results from the small values of the theoretical viscosity near the walls. To obtain the correct values of the shear stress near the walls, the theoretical strain rates must be very large to compensate for the abnormally low theoretical viscosities near the walls.

However, we do not expect the theory or NEMD results for $\eta(z)$ to be accurate very near the walls. There are several reasons for this. First, we have poor statistics for $n(z)$ and other properties within 1σ of the walls due to an absence of molecules in these regions. Second, the assumption made in the theory that the wall atoms are fixed leads to neglect of fluid-wall momentum transfer through motion of the wall atoms. The NEMD results are also subject to uncertainty

very near the wall, due to temperature gradients there (see below).

Because of these difficulties we give a comparison of the velocity profiles with the theoretical streaming velocity matched to the corresponding NEMD velocity in the mid-channel. These are shown in part (b) of Figs. 2–4. The corresponding strain rates are shown in part (c) of Figs. 2–4. We see that, except within about 1.0σ of the walls, the velocities and strain rates agree well. Thus, for the state points and channel widths studied here, theory and simulation agree well in the regions where the theory is expected to be accurate. The high apparent level of “slip” predicted by theory near the walls makes a prediction of the total mass flow

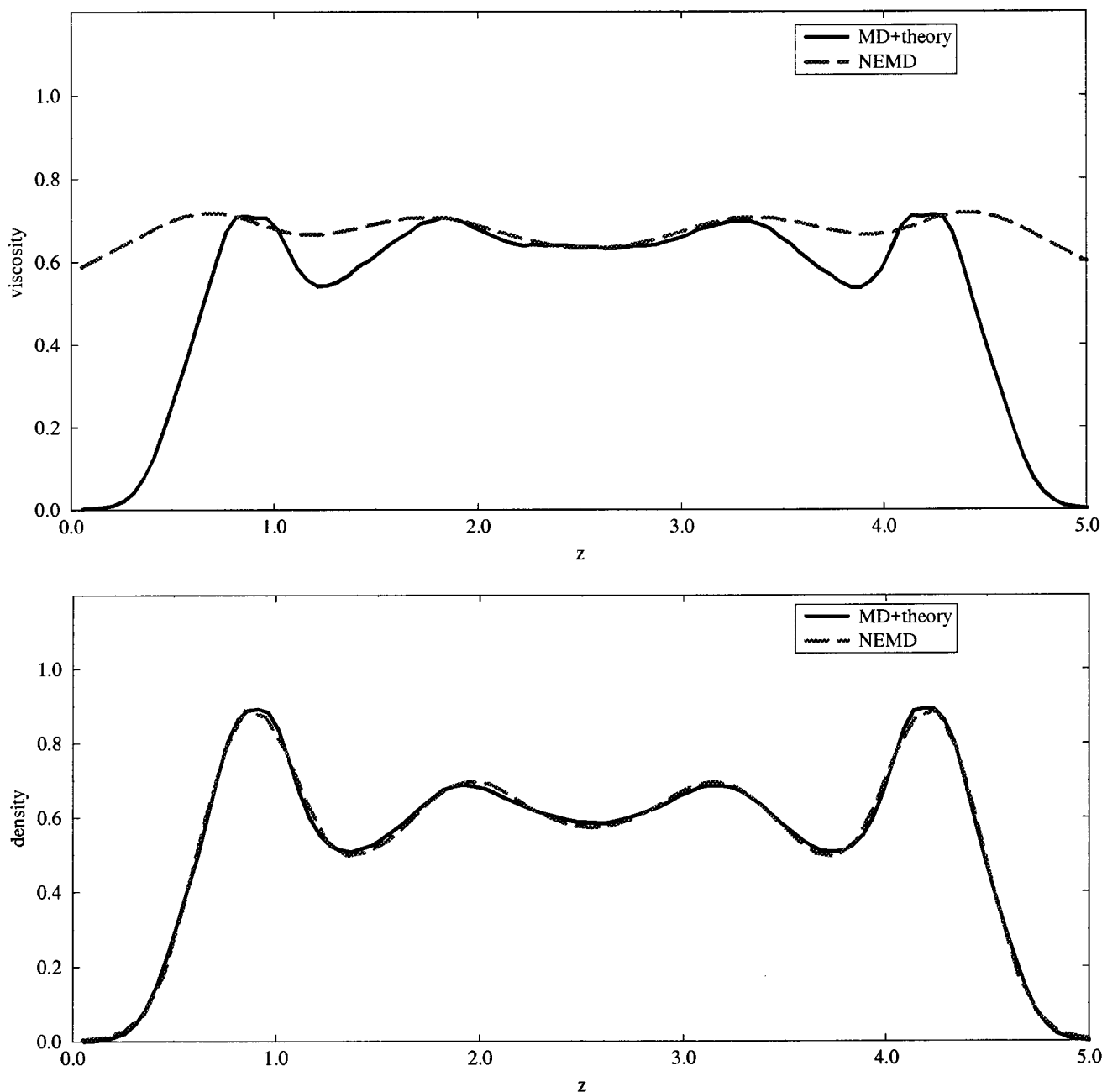


FIG. 9. As for Fig. 5, but for $H=5.1$, $n_{av}=0.522$, $T=0.755$.

across a slit pore by theory rather problematic. Perhaps the easiest way to correct for this difficulty would be to fit the mid-channel theoretical velocity profile to a parabola, ignoring the spurious prediction within 1.0σ of the walls. One could correct the theoretical velocity profile by shifting the fitted parabola so that $u_x(z)=0$ at the walls. This procedure would be quite accurate for the flows studied here. The main practical difficulty in this procedure would be identifying the precise location of the places in the fluid where $u_x(z)=0$. The location of these zero velocity planes suffers from the same difficulty as the identification of the volume which is accessible to the fluid.

Comparisons of theory and NEMD for the density and

viscosity profiles for each of the systems studied are shown in Figs. 5–10. The density profiles are in excellent agreement in each case, indicating that they are little affected by the nonequilibrium state of the flowing system for the conditions studied here. This in turn shows that we are indeed within, or very close to, the linear regime. The viscosities are in good agreement except near the walls. The main disagreement is for the region within 1.0σ of the walls, where as noted the theory predicts that the viscosity goes to zero, while in NEMD it remains finite. Both theory and NEMD results show oscillations in the viscosity near the walls. The theoretically predicted oscillations appear to be larger than those from NEMD.

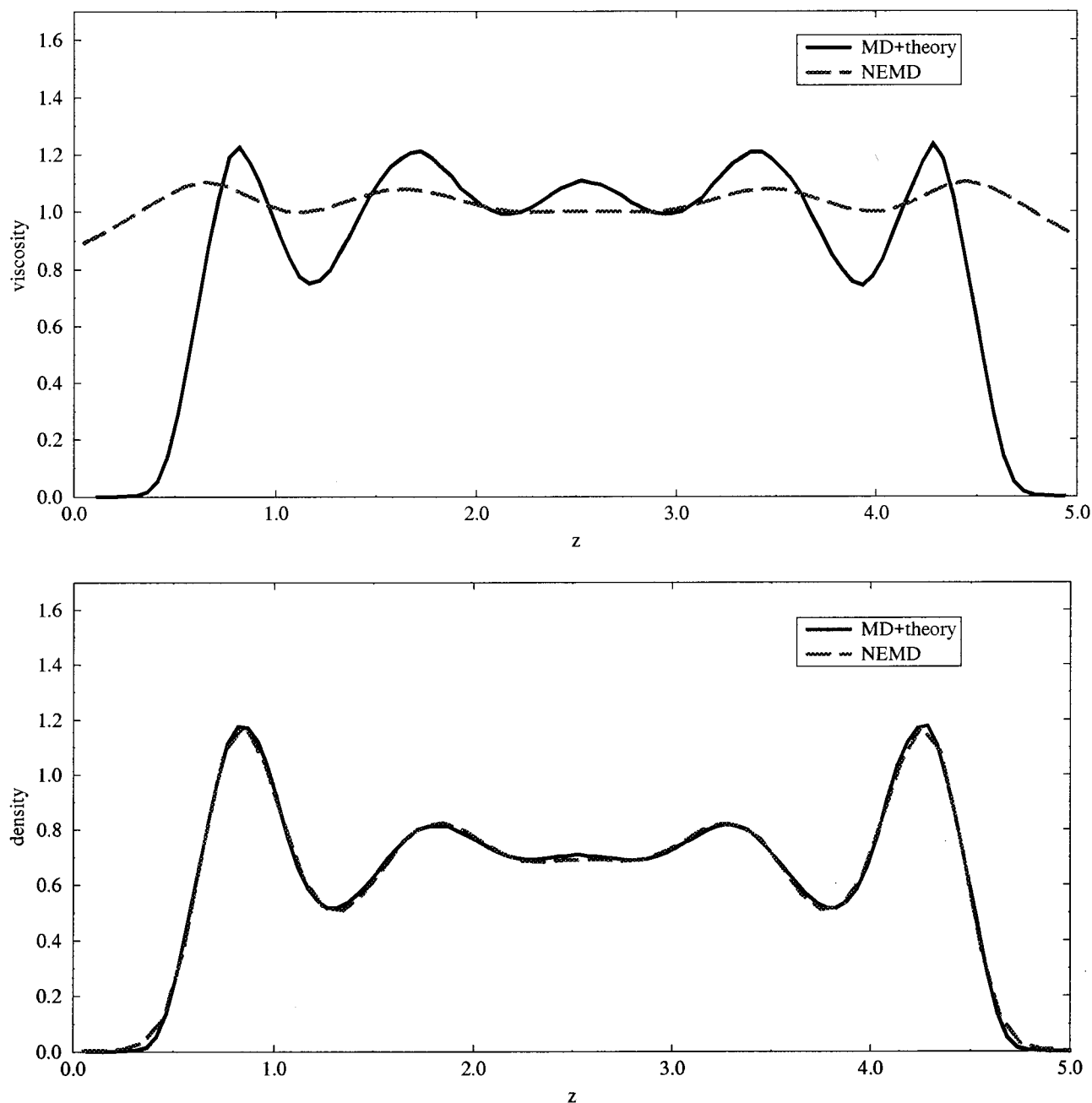


FIG. 10. As for Fig. 5, but for $H=5.1$, $n_{av}=0.603$, $T=0.958$.

Although the wall temperature is maintained at $T=0.722$ in the NEMD simulations, the average temperature in the pore is higher than this (see Table I), raising the question of the importance of temperature gradients in the pore. Temperature profiles were monitored, and it was found that the temperature was constant over the pore except very close to the walls, within $0.3\text{--}0.5\sigma$ of the wall. A typical result is shown in Fig. 11 for a pore of width $H=5.1$. Here $T=0.93$ in the pore, and is essentially constant except within about 0.3σ of the wall, where it falls rapidly to the wall value. It should be noted that each wall consists of three layers, and $T=0.722$ is the wall temperature averaged over the three layers, so that

the temperature in the outermost wall layer may be a little higher than 0.722 .

The NEMD results reported in Figs. 2–11 were for a spring constant K of 160. Some runs were also carried out for a much higher spring constant of $K=1000$ to check on the effect of momentum transfer with the wall. The rms displacement of the wall atoms was 0.0466σ for $K=1000$ and 0.118σ for $K=160$. The density profiles for the two cases were almost identical, with minor differences very near the walls. The higher spring constant led to higher pore temperatures, due to the reduced momentum transfer with the wall.

It is of interest to know how the viscosities in the inner

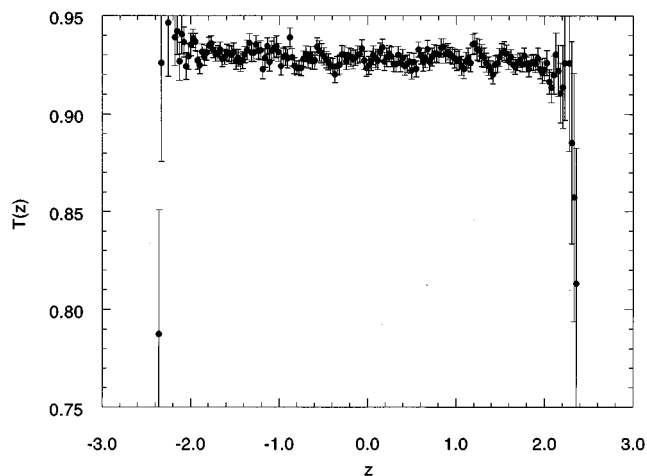


FIG. 11. Typical temperature profile across the pore, $H=5.1$, $n_{\text{av}}=0.60$.

pore region compare with those for a bulk fluid of the same density and temperature. We therefore carried out simulations to determine the bulk viscosities for densities and temperatures corresponding to the runs for the pores of $H=5.1$ (differences between bulk and pore viscosities are expected to be larger for these cases than for $H=20$). The average pore densities listed in Table I are based on a pore volume in which $H=5.1$, and so do not account for the small amount of dead space near the walls. In making the bulk fluid calculations we therefore used an effective average number density, n_{eff} , calculated using a slightly smaller H value obtained by omitting the space near the walls where the local density was effectively zero. For the bulk simulations the standard Gaussian thermostatted SLLOD algorithm¹⁴ was used. The calculations were carried out for a system of 256 molecules at a reduced strain rate of 0.15, which was sufficiently small to give results very close to the zero strain rate values at the densities studied. After equilibration, the calculations were run for a million timesteps with a reduced timestep of 0.001.

The results of these bulk simulations are compared with viscosities in the pores in Table II. The pore viscosities are values averaged over the inner part of the pore. The pore viscosities are higher than the corresponding bulk values, as expected. For the higher densities of $n=0.522$ and 0.603 , this increase in viscosity due to confinement is 43% and 50%, respectively. The theory is seen to successfully reproduce this increase in each case.

V. CONCLUSIONS

The NEMD simulations show that the average viscosity in the pore is greater than that in a bulk liquid at the same

TABLE II. Comparison of viscosities in pores of $H=5.1$ with bulk viscosities at the same effective density, n_{eff} , and temperature. Uncertainty in the viscosity values is estimated to be 0.01.

n	n_{eff}	T	η_{bulk}	η_{pore}	
				NEMD	Theory
0.442	0.451	0.729	0.35	0.41	0.45
0.522	0.533	0.755	0.47	0.67	0.67
0.603	0.615	0.958	0.70	1.05	1.09

temperature and mean density as the pore fluid, by more than 50% for the smaller pores and higher densities. The local viscosity varies across the pore, showing oscillations as the pore wall is approached; for the smaller pores these oscillations in viscosity persist across the entire width of the pore.

The theory of Pozhar and Gubbins is in good agreement with these viscosity results, except for the region within about 1.0σ of the walls. The theory predicts the increase in mean viscosity in the pore well, and also predicts oscillations in local viscosity that are somewhat larger than shown by the NEMD results. The disagreement between theory and NEMD results very near the wall is believed to arise from several factors including: (a) poor statistics near the walls due to the low density of molecules in this region, (b) neglect of contributions to the stress tensor from motion of the wall atoms in the theory, (c) the use of Eq. (20) in place of (19), and (d) temperature gradients near the walls in the NEMD simulations.

The interaction potentials used in this work were purely repulsive. In future work we plan to study the effects of inclusion of attractive fluid–fluid and fluid-wall forces. Fluid-wall attractions, in particular, are likely to have a large effect on the results.

ACKNOWLEDGMENTS

It is a pleasure to thank H. T. Davis and D. Ulberg for helpful discussions. This work was supported by NSF Grant No. CTS-9508680, and also by a NSF US/Australia cooperative research grant (No. INT-9215726). Supercomputer time was provided under a NSF Metacenter Grant (No. MCA93S011P), and utilized the IBM SP2 at the Cornell Theory Center, Cornell University.

- ¹L. A. Pozhar and K. E. Gubbins, *J. Chem. Phys.* **94**, 1367 (1991).
- ²L. A. Pozhar and K. E. Gubbins, *J. Chem. Phys.* **99**, 8970 (1993).
- ³L. A. Pozhar, *Transport Theory of Inhomogeneous Fluids* (World Scientific, Singapore, 1994).
- ⁴H. T. Davis, *Chem. Eng. Comm.* **58**, 413 (1987).
- ⁵H. T. Davis, *J. Chem. Phys.* **86**, 1474 (1987).
- ⁶W. Sung and J. S. Dahler, *J. Chem. Phys.* **80**, 3025 (1984).
- ⁷I. Bitsanis, J. Magda, M. Tirrell, and H. T. Davis, *J. Chem. Phys.* **87**, 1733 (1987).
- ⁸I. Bitsanis, T. K. Vanderlick, M. Tirrell, and H. T. Davis, *J. Chem. Phys.* **89**, 3152 (1988).
- ⁹I. Bitsanis, S. A. Somers, H. T. Davis, and M. Tirrell, *J. Chem. Phys.* **93**, 3427 (1990).
- ¹⁰S. A. Somers and H. T. Davis, *J. Chem. Phys.* **96**, 5389 (1992).
- ¹¹J. G. Powles, S. Murad, and P. V. Ravi, *Chem. Phys. Lett.* **188**, 21 (1992).
- ¹²S. Y. Liem, D. Brown, and J. H. R. Clarke, *Phys. Rev. A* **45**, 3706 (1992).
- ¹³B. D. Todd, D. J. Evans, and P. J. Daivis, *Phys. Rev. E* **52**, (1995).
- ¹⁴D. J. Evans and G. P. Morriss, *Statistical Mechanics of Nonequilibrium Liquids* (Academic, London, 1990).
- ¹⁵M. P. Allen and D. J. Tildesley, *Computer Simulation of Liquids* (Clarendon, Oxford, 1987).
- ¹⁶J. D. Weeks, D. Chandler, and H. C. Andersen, *J. Chem. Phys.* **54**, 5237 (1971).
- ¹⁷J. A. Barker and D. Henderson, *J. Chem. Phys.* **47**, 4714 (1967).
- ¹⁸J. L. Buchanan and P. R. Tumer, *Numerical Methods and Analysis* (McGraw-Hill, New York, 1992).
- ¹⁹K. Wilson, in *Recent Developments in Gauge Theories*, Cargese, 1979 (Plenum, New York, 1980).
- ²⁰H. Flyvbjerg and H. G. Peterson, *J. Chem. Phys.* **91**, 1 (1989).